

Tunable Bandgap in Silicene and Germanene

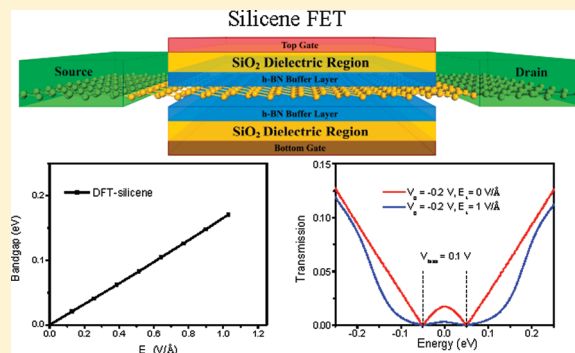
Zeyuan Ni, Qihang Liu, Kechao Tang, Jiaxin Zheng, Jing Zhou, Rui Qin, Zhengxiang Gao, Dapeng Yu, and Jing Lu*

State Key Laboratory of Mesoscopic Physics, Department of Physics, Peking University, Beijing 100871, P. R. China

S Supporting Information

ABSTRACT: By using ab initio calculations, we predict that a vertical electric field is able to open a band gap in semimetallic single-layer buckled silicene and germanene. The sizes of the band gap in both silicene and germanene increase linearly with the electric field strength. Ab initio quantum transport simulation of a dual-gated silicene field effect transistor confirms that the vertical electric field opens a transport gap, and a significant switching effect by an applied gate voltage is also observed. Therefore, biased single-layer silicene and germanene can work effectively at room temperature as field effect transistors.

KEYWORDS: Silicene, germanene, band gap, quantum transport, electric field, first-principles calculation



Graphene has attracted great interest recently for its exceptional electronic properties.^{1–4} For instance, its charge carriers are massless Dirac fermions, leading to a mobility up to $15\,000\text{ cm}^2\text{ V}^{-1}\text{ s}^{-1}$ for graphene on SiO_2 substrate and $200\,000\text{ cm}^2\text{ V}^{-1}\text{ s}^{-1}$ for suspended sample.^{1–4} However, the promising application of graphene in present electronic devices, like field effect transistor (FET), still relies on the opening and controlling of the band gap. Although a band gap is opened in bilayer and multilayer graphene under an external vertical electric field due to the inversion symmetry breaking,^{5–9} monolayer graphene remains zero-gap semimetallic because its two sublattices remain equivalent under an external vertical electric field. Consequently, biased monolayer graphene cannot be operated effectively as a FET at room temperature. Other group IV elements, such as silicon and germanium, also have stable honeycomb monolayers (namely silicene and germanene).^{10,11} Synthesis of pristine,¹² Mg-doped¹³ and hydrogenated¹⁴ silicene, and pristine silicene nanoribbon¹⁵ have been reported. Unlike planar graphene monolayers, the most stable silicene and germanene monolayers prefer a low-buckled (LB) structure^{10–12} (silicene and germanene referred to in the following are those with LB structure). The electronic structures of the silicene and germanene are quite similar to that of graphene.^{10,11} Namely, silicene and germanene are zero-gap semimetallic, and their charge carriers are also massless fermions because their π and π^* bands are linear at the Fermi level (E_f). When a vertical electric field is applied, the atoms in a buckled structure are no longer equivalent, and a band gap opening may become possible in silicene and germanene. If so, one can fabricate an FET operating at room temperature out of pure silicene and germanene.

In this Letter, we investigate the effects of a vertical electric field on silicene and germanene by means of the density functional theory (DFT) and the nonequilibrium Green's function (NEGF) method.

A band gap is unambiguously opened, and its size and the effective carrier mass increase linearly with the electric field strength. The effects of the vertical electric field on the transport properties of silicene are subsequently examined by fabricating a prototype of dual-gated silicene FET. A transport gap induced by perpendicular electric field is found, accompanied by significant switching effects by gate voltage.

Geometry optimization and electronic structure are calculated by using an all-electron double numerical atomic basis set plus polarization (DNP), as implemented in the Dmol³ package.¹⁶ A $32 \times 32 \times 1$ Monkhorst–Pack¹⁷ k -points grid is used in the first Brillouin zone sampling. A vacuum space of 20 \AA is placed to avoid interaction between the monolayer and its periodic images. Both the atomic positions and lattice constant are relaxed. Transportation properties are calculated by the DFT coupled with NGEF formalism implemented in the ATK 11.2 package.^{18–20} Both single- ζ (SZ) and double- ζ plus polarization (DZP) basis sets are employed. The k -points of the electrodes and central region, which are generated by the Monkhorst–Pack scheme as well, are set to $1 \times 300 \times 300$ and $1 \times 300 \times 1$, respectively. The temperature is set to 300 K . The current is calculated by using the Landauer–Büttiker formula:²¹

$$I(V_g, V_{\text{bias}}) = \frac{2e}{h} \int_{-\infty}^{+\infty} \{T_V(E, V_{\text{bias}})[f_L(E - \mu_L) - f_R(E - \mu_R)]\} dE \quad (1)$$

where $T_V(E, V_{\text{bias}})$ is the transmission probability at a given gate voltage V_g and bias voltage V_{bias} , $f_{L/R}$ the Fermi–Dirac

Received: September 4, 2011

Revised: October 31, 2011

Published: November 03, 2011

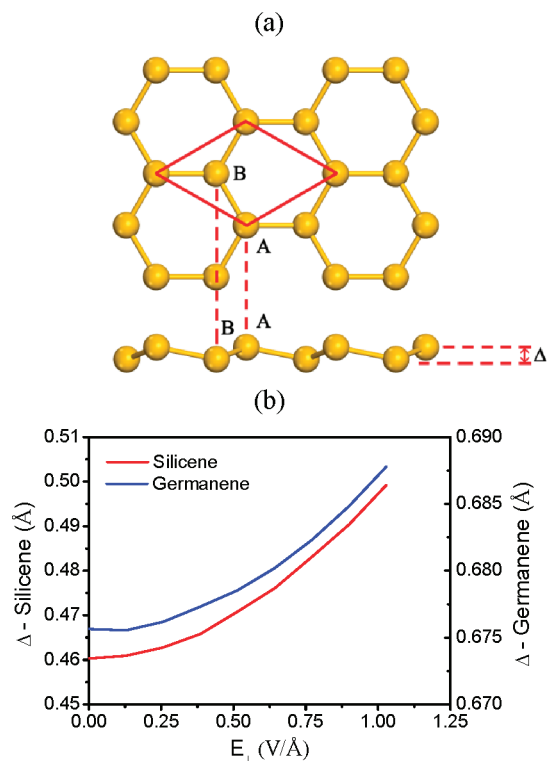


Figure 1. (a) Top and side view of silicene monolayer. The primitive cell is denoted by the red rhombus. The two equivalent atoms in silicene, labeled as A and B, respectively, have a corrugated arrangement. The structure of germanene is almost the same, except for a slightly larger lattice constant and buckling distance. (b) Buckling distance Δ of silicene and germanene as a function of E_{\perp} calculated at the GGA/DNP level. The left scale is for silicene, and the right one is for germanene.

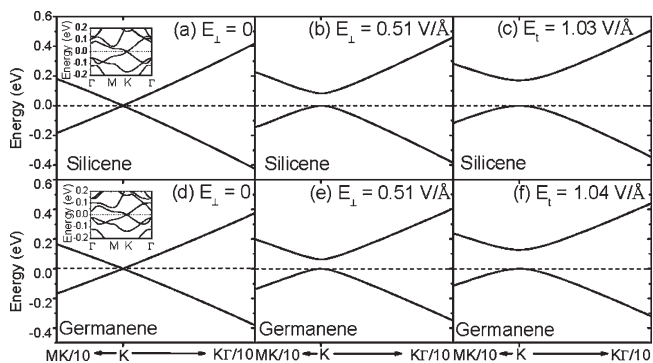


Figure 2. Band structures of (a–c) silicene and (d–f) germanene around E_f at three different vertical electric fields calculated at the GGA/DNP level. Inset in (a) and (d): Band structures in the first Brillouin zone at $E_{\perp} = 0$. The Fermi level or the valence band top is set to zero.

distribution function for the left (L)/right (R) electrode, and μ_L/μ_R the electrochemical potential of the L/R electrode. Effects of gate are calculated by solving the Poisson equation self-consistently instead of simply lifting the central region’s chemical potential. A generalized gradient approximation (GGA) to the exchange–correlation functional, of the Perdew–Burke–Ernzerhof (PBE) form,²² is used throughout this paper, unless otherwise specified.

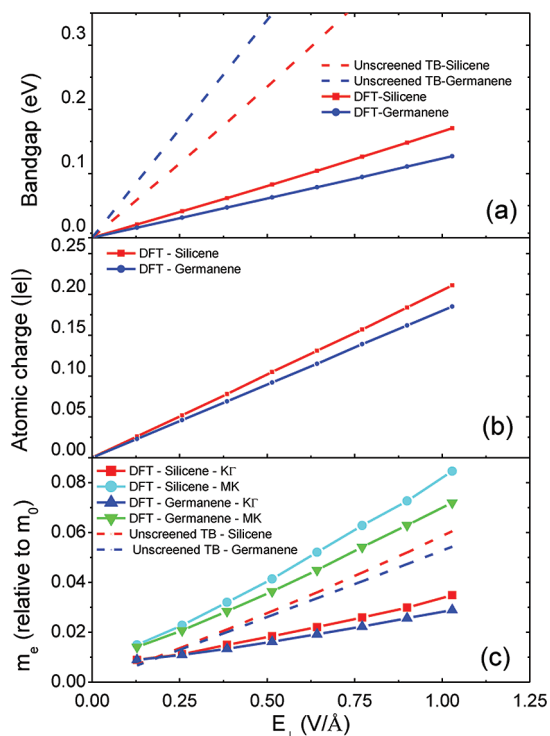


Figure 3. (a) Band gap, (b) Mulliken charge transferred from one equivalent atom to the other, and (c) effective mass of electron at the conduction band bottom along the KΓ and MK directions of silicene and germanene as a function of vertical electric field calculated at the GGA/DNP level. The coupling coefficient of nearest neighbors in the TB model is set to 1.7 eV in silicene and 2.0 eV in germanene.

The optimized electric field free silicene (shown in Figure 1a) and germanene at the GGA/DNP level have lattice constants of $a = 3.866$ and 4.063 Å, respectively. The corresponding buckling distances are $\Delta = 0.460$ and 0.676 Å, respectively. These structural parameters are in good agreement with previous works.^{10,11,23} As displayed in Figure 1b, the Δ value increases monotonically and nonlinearly with E_{\perp} after the application of a vertical electric field, with an increment of 3%/0.2% at $E_{\perp} = 0.51$ V/Å and 8%/0.8% at $E_{\perp} = 1.03$ V/Å in silicene/germanene. The changes in the lattice constant a are less than 0.2% in both silicene and germanene under $E_{\perp} = 0$ –1.03 V/Å. Figure 2a–f shows the band structures of silicene and germanene under three different electric field E_{\perp} . Their conduction and valence bands touch linearly at the K point when $E_{\perp} = 0$; thus, both silicene and germanene are semimetals with zero gap and zero effective mass. However, when finite E_{\perp} is applied to silicene and germanene, a direct band gap is opened at the K point. The opened band gap is $E_g = 0.08/0.06$ eV for silicene/germanene under $E_{\perp} = 0.51$ V/Å and doubled under $E_{\perp} = 1.03$ V/Å. The finer response of the band structure to E_{\perp} of silicene is provided in Figure S1, Supporting Information. As shown in Figure 3a, the opened band gap increases linearly with E_{\perp} and surpasses the room temperature scale (0.026 eV) at $E_{\perp} = 0.16$ V/Å. The electric field required to open a gap of 0.16 eV in silicene and germanene is greater than that in bilayer and multilayer graphene by about an order of magnitude, but the band gaps in the latter increase nonlinearly with E_{\perp} and are saturated around $E_{\perp} = 0.1$ V/Å.^{7–9} Considering the sizable underestimation of the band gap in conventional DFT for a low-dimensional semiconductor,^{24,25} the

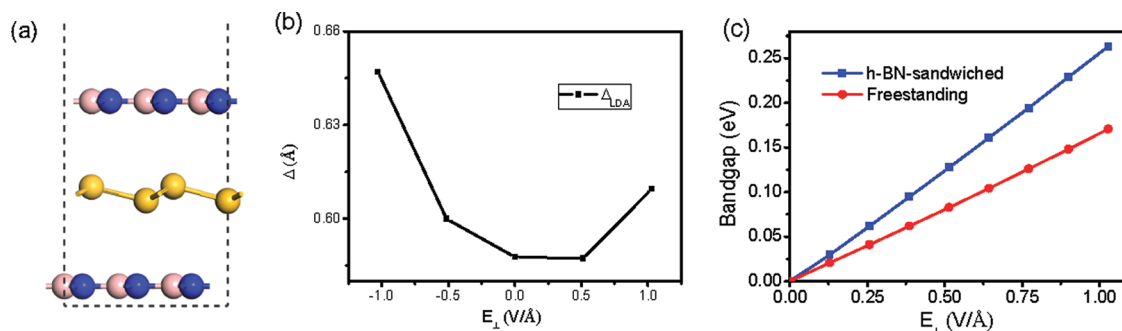


Figure 4. (a) Relaxed h-BN-sandwiched silicene at zero electric field and (b) buckling and (c) bandgap as a function of vertical electric field E_{\perp} for silicene sandwiched between h-BN single layers. The sandwich structure is relaxed using the local density approximation (LDA) to the exchange–correlation functional with the DZP basis set because it fortunately better predicts the interlayer distance than the GGA, while the band structures are calculated at the GGA/DNP level. The bandgap dependence of freestanding silicene on E_{\perp} is also shown for comparison. The three layers are randomly stacked, and the sandwich structure with AA stacked h-BN is also examined, and there is no significant difference in bandgap– E_{\perp} relationship from the above result.

real band gaps in silicene and germanene should be significantly greater than the GGA/DNP ones. The MIN basis set yields a 4% larger lattice constant and 60–70% larger buckling (see Figure S2a, Supporting Information) than the DNP results and other theoretical values^{10,11,23} and thus unreliable in structural determination. However, the bandgap calculated with the MIN basis set based on the DNP (equivalent to DZP) optimized silicene structure is only 20% larger than those with the DNP basis set (see Figure S2b, Supporting Information).

The linear dependence of E_g on E_{\perp} is well explained in terms of a tight binding (TB) model calculation (see Supporting Information), which gives $E_g = eE_{\perp}\Delta$, and the result is shown as the dashed lines in Figure 3a. The band gaps of the TB model are several times larger than those of DFT because the screening effect is not taken into account in our TB model. Mulliken population analysis displays a net charge transfer from one atom to the other in the primitive cells of silicene and germanene (shown in Figure 3b), and the amount of the polarized charge increases linearly with E_{\perp} . Therefore screening effect exists and is enhanced with E_{\perp} . According to the TB model, silicene has a smaller Δ and thus has a smaller E_g than germanene, while in the DFT calculation silicene has a larger E_g . Although the polarized charge in silicene is larger than that in germanene, it does not mean that silicene's screening is greater than germanene's, because Mulliken population analysis is rough and incapable of taking the charge's spatial distribution into account. In fact, bulk germanium has a larger dielectric constant ($\epsilon = 16.0$) and therefore more powerful screening effect than silicon ($\epsilon = 11.9$) does. In our self-consistent DFT calculation, the larger screening effect in germanium leads to a smaller band gap in germanene compared with silicene.

The variations of effective carrier masses of silicene and germanene along several directions in k -space under electric field are investigated by quadratic polynomial fitting of the conduction and valence bands (see Supporting Information). The effective masses of the conduction band bottom of silicene and germanene along the MK (m_e^{MK}) and K Γ ($m_e^{\text{K}\Gamma}$) are plotted in Figure 3c. The m_e^{MK} values of silicene and germanene are larger than their respective $m_e^{\text{K}\Gamma}$. All the four effective masses have an approximately linear relationship with E_{\perp} , and the linear dependence of the effective m_e on E_{\perp} remains in other directions we checked. Such a linear relationship of m_e on E_{\perp} is also well explained in terms of the TB model (dashed lines in Figure 3c).

The latter gives an isotropic effective electron mass (see Supporting Information): $m_e = (2\hbar^2 E_{\perp} e \Delta) / (3a^2 \gamma_1^2)$, where γ_1 is the nearest neighbors' coupling coefficient. The effective mass of the valence band top (m_h) is almost the same as that of the respective m_e with a difference within 2% in DFT and is exactly the same in the TB model due to the symmetrical band structure around E_f in silicene and germanene. At $E_{\perp} = 0.4$ V/Å, effective masses in silicene ($m_e^{\text{K}\Gamma} = 0.015 m_0$, $m_e^{\text{MK}} = 0.033 m_0$, where m_0 is the free electron mass) and germanene ($m_e^{\text{K}\Gamma} = 0.014 m_0$, $m_e^{\text{MK}} = 0.029 m_0$) monolayers are compared with those in electric field free bilayer graphene ($m_e^{\text{K}\Gamma} = 0.028 m_0$, $m_h^{\text{K}\Gamma} = 0.029 m_0$, $m_e^{\text{MK}} = 0.012 m_0$, and $m_h^{\text{MK}} = 0.015 m_0$).⁹ Mobility μ and effective carrier mass m^* have a simple relation: $\mu = e\tau/m^*$. In light of the fact that suspended graphene has a mobility of $\mu \sim 200\,000$ cm² V⁻¹ s⁻¹,^{1–4} the mobilities of suspended silicene and germanene under $E_{\perp} = 0.4$ V/Å are estimated to be on the order of 10^5 cm² V⁻¹ s⁻¹, if the scattering time τ is similar between graphene and silicene/germanene.

In light of the reactive nature of sp³ hybridized silicene, the dielectric should be carefully chosen. Experimentally, graphene has been deposited on an inactive hexagonal boron nitride (h-BN) multilayer, and the mobility of graphene is elevated by 1 order of magnitude compared with an SiO₂ substrate-supported sample due to the smooth surface of h-BN.^{26,27} It is suggested that preservation of a high mobility in a dual-gated graphene device may be achieved by fabricating an h-BN/graphene/h-BN stack using a two-transfer technique.²⁶ Theoretical investigation of h-BN/graphene/h-BN sandwich structure shows that electrical field-induced bandgap opening in bilayer graphene is nearly unaffected by h-BN.²⁸ Our simulation shows that silicene will spontaneously form covalent bonds with both Si and O atoms on the common SiO₂ dielectric (Figure S3, Supporting Information). However, both silicene and h-BN are approximately intact when placed on or sandwiched between h-BN even under an electric field of up to 2 V/Å. Total energy of silicene/h-BN system as a function of the distance between silicene and h-BN is provided in Figure S4, Supporting Information, with an equilibrium distance of 3.30 Å between silicene and h-BN. Figure 4a shows the sandwich structure under zero electric field. The buckling of silicene placed on (Figure S5, Supporting Information) or sandwiched between (Figure 4b) h-BN is also slightly enhanced by E_{\perp} . The bandgap of silicene sandwiched between h-BN is even larger by 50% than that of freestanding

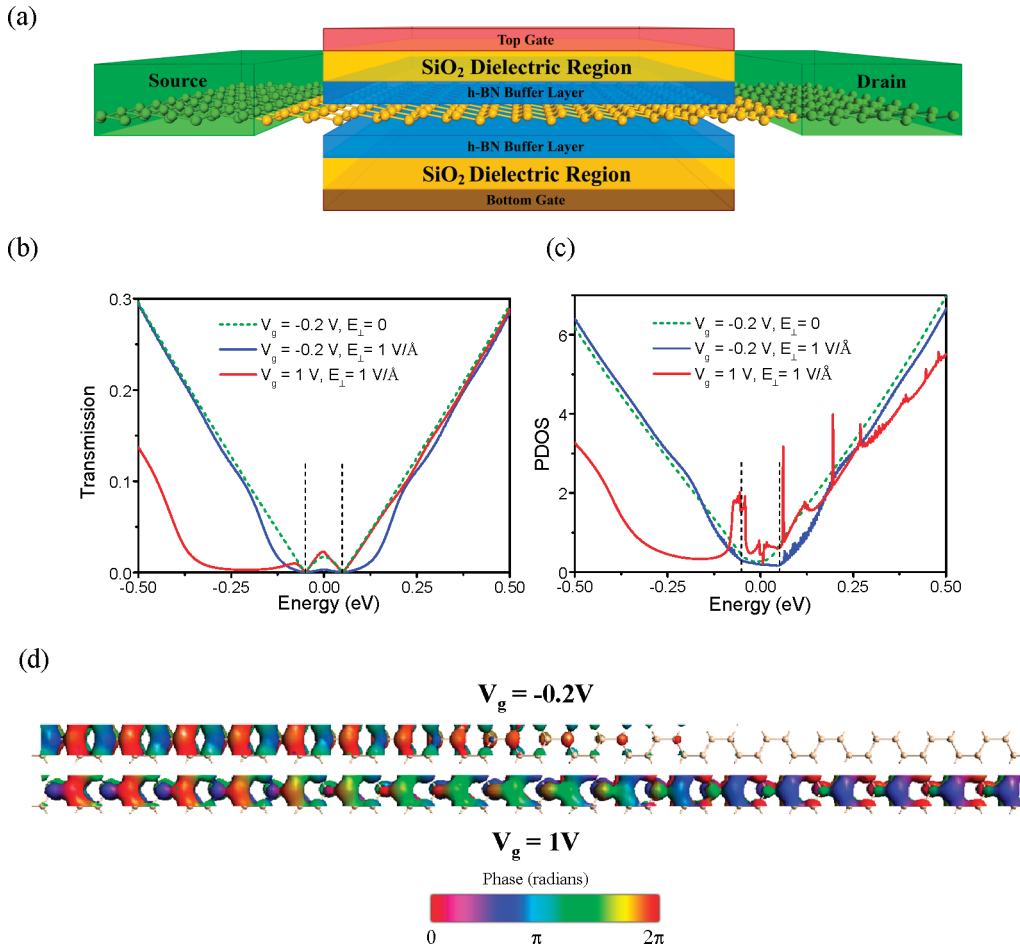


Figure 5. Dual-gated silicene FET: (a) schematic model, (b) transmission spectra, and (c) projected density of states of the channel under different gate voltages and electric fields with a fixed $V_{\text{bias}} = 0.1$ V, obtained from the GGA/SZ level. The dashed vertical line indicates the bias window. The channel length is ~ 67 Å. The Fermi level is set to zero. (d) Transmission eigenstates for the off- and on-state ($V_g = -0.2$ and 1 V, respectively) at E_{\perp} and at the $(0, 1/3)$ point of k -space under $E_{\perp} = 1$ V/Å. The isovalues are 0.8 au.

silicene under the same E_{\perp} (see Figure 4c). Therefore, insertion of h-BN buffer layer between silicene and oxide substrate is strongly recommended in a silicene FET device to maintain the structural integrity and high carrier mobility. In the dual-gated silicene FET, silicene should be sandwiched between h-BN buffer layers. Our simulation shows that even single layer h-BN is nearly flat on SiO_2 surface (Figure S6, Supporting Information) (multilayer h-BN is more robust against buckling); therefore the structure of silicene sandwiched between h-BN buffer layer can be maintained when placed on SiO_2 dielectric.

The model of a dual-gated silicene FET with SiO_2 dielectric and h-BN buffer layer is shown in Figure 5a. Different from a single-gated FET, a dual-gated device can control not only the doping level but also the vertical electric field applied to the monolayer. The top and bottom gate voltages are labeled by V_t and V_b , respectively. The distance between the two gates is $d_0 = 20$ Å in our model, and the thickness of the both top and bottom dielectric plus buffer regions is $d_i = 7$ Å. To avoid an insulator-to-metal transition in few-layer h-BN caused by the Stark effect and to ensure the system can endure a strong electric field, the number of layers of buffer h-BN should be limited according to the DFT calculations.^{29,30} According to the DFT calculations, h-BN trilayer remains semiconducting under $E_{\perp} = 0.8$ ²⁹ or 1 V/Å³⁰ and can be used as buffer layer working under a strong

electric field up to $0.8\text{--}1$ V/Å, since h-BN trilayer probably can effectively prevent a tunneling between the gate and silicene. The dielectric constant of the dielectric and buffer regions is taken as $\epsilon = 3.9$, which models SiO_2 and h-BN ($\epsilon = 3\text{--}4$). The vertical electric field applied to a silicene can be written as $E_{\perp} = (V_t - V_b)/(d_0 - 2d_i + 2d_i/\epsilon)$. The corresponding total gate voltage is $V_g = V_t + V_b$, reflecting the total doping level.

The transmission spectra of the device with a channel length of ~ 67 Å under different E_{\perp} and V_g using an SZ basis set are displayed in Figure 5b, where the bias voltage is fixed at $V_{\text{bias}} = 0.1$ V. As we know, the total conductance $G(E_{\perp}, V_g)$ of an FET is proportional to the projected density of states (PDOS) of electrodes (denoted as $D_L(E_{\perp}, V_g)$ for the left one and $D_R(E_{\perp}, V_g)$ for the right one) and the channel cell (denoted as $D_C(E_{\perp}, V_g)$):^{31,32}

$$G(E_{\perp}, V_g) \propto \frac{D_L(E_{\perp}, V_g)D_C(E_{\perp}, V_g)D_R(E_{\perp}, V_g)}{D_L(E_{\perp}, V_g)D_R(E_{\perp}, V_g) + D_L(E_{\perp}, V_g)D_C(E_{\perp}, V_g) + D_R(E_{\perp}, V_g)D_C(E_{\perp}, V_g)} \quad (2)$$

if the device is considered to be three resistors in series. Under $V_{\text{bias}} = 0.1$ V, the Dirac points of the source and drain in silicene FET move to ± 0.05 eV, respectively, regardless of E_{\perp} and V_g .

Under zero vertical electric field, there is a transmission “bulge” around E_f inside the bias window at $V_g = -0.2$ V for both the SZ (Figure 5b) and DZP (Figure S7, Supporting Information) basis sets. This is exactly as the case of graphene,³² in which the relatively large transmission coefficients inside the bias window (i.e., the “bulge”) lead to a relatively large current. However, upon the application of $E_{\perp} = 1$ V/Å on silicene, an obvious transport gap of about 0.14 eV is opened (Figure 5b) due to the occurrence of an about 0.12 eV pseudogap in $D_C(E_{\perp}, V_g)$ (Figure 5c) with an SZ basis set used, which apparently originates from the band gap of periodic silicene under the same E_{\perp} . The channel PDOS pseudogap and the transport gap can be shifted by V_g (Figure 5b, c and Figures S8 and S9, Supporting Information). Under $V_g = 1$ V, both the two gaps are moved away from the bias window, resulting in the recovery of the bulge, and the device is turned from off- to on-state. $V_g = -0.2$ V is chosen to represent the off-state instead of $V_g = 0$ since the former case has smaller current, owing to the asymmetry of the transport gap around E_f . The difference in the off- and on-state is reflected from the transmission eigenchannel at E_f and at the (0, 1/3) point of k -space, as displayed in Figure 5d. The transmission eigenvalue of the off-state is 0.09, and the corresponding incoming wave function is apparently scattered and unable to reach to the other lead. On the contrary, the transmission eigenvalue of the on-state is 0.87, in which case the scattering is weak, and most of the incoming wave is able to reach to the other lead. The on/off current ratio under $E_{\perp} = 1$ V/Å is 4.2 with the SZ basis set at 300 K. When a larger DZP basis set is used, a smaller pseudogap of about 0.1 eV in the transmission spectrum is opened under $E_{\perp} = 1$ V/Å (Figure S7, Supporting Information), and the on/off current ratio is reduced to 1.7.

The current switch effects in vertically biased silicene are much weaker when compared with a traditional MOSFET, where the bandgap is more than 0.4 eV and the on/off ratio is 10^4 – 10^7 .³³ The first cause is the use of a rather short channel (~ 67 Å), which gives rise to a larger leakage current in the off-state due to tunneling. Previous ab initio transport simulations^{34,35} have shown that on/off ratio increases apparently with the channel length for a graphene nanoribbon and carbon nanotube due to the reduced current leakage in the off-state (namely short channel effect). For examples, when the channel length of a graphene nanoribbon-based FET is increased from 17 to 68 Å, the on/off ratio is raised by a factor of 10^4 ,³⁴ and when the channel length of a functionalized single-walled carbon nanotube based FET is increased from 22 to 66 Å, the on/off ratio is increased by a factor of 10^5 .³⁵ In our case, when the channel length of silicene is increased from 67 Å by a factor of 1.5 at $E_{\perp} = 1$ V/Å, the on/off ratio is increased to 7.4 (SZ) and 2.2 (DZP) (Figure S10, Supporting Information), respectively. When the channel length is further increased by a factor of 1.9 at $E_{\perp} = 1$ V/Å, the on/off ratio is increased to 8.3 (SZ) and 2.6 (DZP). A larger on/off ratio is expected if the channel length is further increased and the device is further optimized.

Second, it is well-known that the conventional DFT has a tendency to underestimate the bandgap a semiconductor and that a quasiparticle correction (GW method) is required to obtain a reliable bandgap. Taking bulk Si as an example, the bandgap correction is increased by a factor of 150% upon quasiparticle correction. Such a bandgap correction is generally enhanced when dimensionality is reduced,^{24,36} and the bandgap correction in 2D silicene is expected to be greater (over 150%) than the correction in bulk silicon. The bandgap of silicene under

$E_{\perp} = 2$ V/Å is twice that under $E_{\perp} = 1$ V/Å and is chosen here as an approximation of the GW bandgap under $E_{\perp} = 1$ V/Å. Compared the case with $E_{\perp} = 1$ V/Å, the PDOS and transmission spectra are further depressed near E_f at $E_{\perp} = 2$ V/Å, as shown in Figures S7 and S8, Supporting Information. The DFT on/off ratio of a 67 Å channel FET under $E_{\perp} = 2$ V/Å is 50 with an SZ basis set, and the on/off ratio under $E_{\perp} = 1$ V/Å is thus estimated to be 50 upon GW correction. By sharp contrast, the current change ratio is only 1.07 (DZP) \sim 1.12 (SZ) for silicene without a vertical electric field. Hence, a current switching effect induced by perpendicular electric field is well established in our dual-gated silicene FET model.

Finally, we must point out that simply obtaining a large on/off ratio of silicene and graphene is not very difficult. For example, by cutting graphene into a nanoribbon, the on/off ratio can reach 10^6 .³⁷ However, one thing must be kept in mind that one of the most striking merits of silicene and graphene is their extraordinary high carrier mobility, which is 1–2 orders higher compared to a Si semiconductor and can lead to a quicker switching speed. It is a great challenge to simultaneously obtain high on/off ratio and keep ultrahigh carrier mobility in silicene and graphene, because the switching effect usually increases with the bandgap whereas the mobility usually decreases with the bandgap. The available methods to obtain a high on/off ratio in graphene always lead to a drastic decrease in the carrier mobility by several orders of magnitude, totally losing the mobility advantage of graphene. If we want to maintain the extremely high carrier mobility of silicene and graphene, we have to compromise on the switching effect. Actually, as a feasible way to open a bandgap of bilayer graphene up to 0.25 eV⁷ without loss in carrier mobility, the measured room-temperature on/off ratio in a vertically biased bilayer graphene FET is only increased by a factor of 25 than that of the unbiased one.³⁸ In our work, the enhancement factor of vertically biased silicene with respect to the unbiased one is 8 (when the SZ basis set and a 130 Å long channel are used) to 50 (with possible GW correction and 67 Å long channel). Such enhancements are encouraging because the opened bandgap of silicene under an electric field of 1 V/Å is only half the maximum bandgap (0.25 eV) of bilayer graphene opened by an electric field, and the extremely high mobility of silicene ($\mu \sim 10^4$ – 10^5 cm² V⁻¹ s⁻¹ in terms of our previous estimation of $\mu \sim 10^5$ cm² V⁻¹ s⁻¹ at $E_{\perp} = 0.4$ V/Å and the relation of $m^* \propto E_{\perp}$ shown in Figure 3C and also derived in the Supporting Information) is maintained simultaneously.

In summary, our ab initio calculations reveal one prominent advantage of silicene and germanene monolayers over a graphene monolayer. Namely, it is possible to open a bandgap in semimetallic low-bulked silicene and germanene monolayers via an external vertical electric field, while it is impossible in a semimetallic planar graphene monolayer. The bandgap and effective masses of both electrons and holes increase linearly with the electric field strength. An electrical field-induced transport gap is calculated in a simulated dual-gated silicene FET device, which enables us to switch the current of such a silicene-based device. Our work is expected to stimulate the experimental fabrication of FET out of pristine silicene and germanene monolayers.

■ ASSOCIATED CONTENT

S Supporting Information. Detailed derivation of electric field-induced band gaps and effective masses by TB, band structures of silicene near the K point under nine different

electric fields, comparison of silicene's buckling and electric-field-induced band gap of silicene using the MIN and DNP basis sets, geometry of silicene on SiO₂ (100) surfaces and h-BN, total energy of silicene on h-BN as a function of the distance between them, effect of electric field on the buckling of silicene in the sandwich structure, optimized single layer h-BN on the O- and Si-terminated SiO₂ (100) surfaces, transmission spectra of the silicene FET with a DZP basis set, PDOS of the channel atoms in the silicene FET under a larger electric field of $E_{\perp} = 2 \text{ V/\AA}$, shift of the zero-bias transmission spectrum of the silicene FET under gate voltages, and transmission spectra of the silicene FET with a 100-Å-long channel. This material is available free of charge via the Internet at <http://pubs.acs.org>.

AUTHOR INFORMATION

Corresponding Author

*E-mail: jinglu@pku.edu.cn.

ACKNOWLEDGMENT

This work was supported by the NSFC (grant no. 10774003), National 973 Projects (no. 2007CB936200, MOST of China), Fundamental Research Funds for the Central Universities, National Foundation for Fostering Talents of Basic Science (no. J0630311), and Program for New Century Excellent Talents in University of MOE of China. We thank Prof. Daniel Wilkins and Prof. Waining Mei for reading this manuscript carefully.

REFERENCES

- Novoselov, K. S.; Geim, A. K.; Morozov, S. V.; Jiang, D.; Zhang, Y.; Dubonos, S. V.; Grigorieva, I. V.; Firsov, A. A. *Science* **2004**, *306*, 666–669.
- Novoselov, K. S.; Geim, A. K.; Morozov, S. V.; Jiang, D.; Katsnelson, M. I.; Grigorieva, I. V.; Dubonos, S. V.; Firsov, A. A. *Nature* **2005**, *438*, 197–200.
- Geim, A. K.; Novoselov, K. S. *Nat. Mater.* **2007**, *6*, 183–191.
- Morozov, S. V.; Novoselov, K. S.; Katsnelson, M. I.; Schedin, F.; Elias, D. C.; Jaszczak, J. A.; Geim, A. K. *Phys. Rev. Lett.* **2008**, *100*, 016602.
- Castro, E. V.; Novoselov, K. S.; Morozov, S. V.; Peres, N. M. R.; Dos Santos, J.; Nilsson, J.; Guinea, F.; Geim, A. K.; Neto, A. H. C. *Phys. Rev. Lett.* **2007**, *99*, 216802.
- Mak, K. F.; Lui, C. H.; Shan, J.; Heinz, T. F. *Phys. Rev. Lett.* **2009**, *102*, 256405.
- Zhang, Y. B.; Tang, T. T.; Girit, C.; Hao, Z.; Martin, M. C.; Zettl, A.; Crommie, M. F.; Shen, Y. R.; Wang, F. *Nature* **2009**, *459*, 820–823.
- Min, H.; Sahu, B.; Banerjee, K. S.; MacDonald, A. H. *Phys. Rev. B* **2007**, *75*, 155115.
- Tang, K. C.; Qin, R.; Zhou, J.; Qu, H. R. G.; J., Z.; Fei, R. X.; Li, H.; Zheng, Q. Y.; Gao, Z. X.; Lu, J. *J. Phys. Chem. C* **2011**, *115*, 9458–9464.
- Cahangirov, S.; Topsakal, M.; Akturk, E.; Sahin, H.; Ciraci, S. *Phys. Rev. Lett.* **2009**, *102*, 236804.
- Sahin, H.; Cahangirov, S.; Topsakal, M.; Bekaroglu, E.; Akturk, E.; Senger, R. T.; Ciraci, S. *Phys. Rev. B* **2009**, *80*, 155453.
- Lalmi, B.; Oughaddou, H.; Enriquez, H.; Kara, A.; Vizzini, S.; Ealet, B.; Aufray, B. *Appl. Phys. Lett.* **2010**, *97*, 223109.
- Nakano, H.; Mitsuoka, T.; Harada, M.; Horibuchi, K.; Nozaki, H.; Takahashi, N.; Nonaka, T.; Seno, Y.; Nakamura, H. *Angew. Chem.* **2006**, *118*, 6451–6454.
- Okamoto, H.; Kumai, Y.; Sugiyama, Y.; Mitsuoka, T.; Nakanishi, K.; Ohta, T.; Nozaki, H.; Yamaguchi, S.; Shirai, S.; Nakano, H. *J. Am. Chem. Soc.* **2010**, *132*, 2710–2718.

- Le Lay, G.; Aufray, B.; Leandri, C.; Oughaddou, H.; Biberian, J. P.; De Padova, P.; Davila, M. E.; Ealet, B.; Kara, A. *Appl. Surf. Sci.* **2009**, *256*, 524–529.
- Delley, B. *J. Chem. Phys.* **1990**, *92*, 508–517.
- Monkhorst, H. J.; Pack, J. D. *Phys. Rev. B* **1976**, *13*, 5188–5192.
- ATOMISTIX Toolkit, version 11.2; QuantumWise A/S: Copenhagen, Denmark, 2011; <http://www.quantumwise.com>.
- Taylor, J.; Guo, H.; Wang, J. *Phys. Rev. B* **2001**, *63*, 121104.
- Brandbyge, M.; Mozos, J. L.; Ordejon, P.; Taylor, J.; Stokbro, K. *Phys. Rev. B* **2002**, *65*, 165401.
- Datta, S. *Electronic Transport in Mesoscopic systems*; Cambridge University Press: Cambridge, England, 1995.
- Perdew, J. P.; Burke, K.; Ernzerhof, M. *Phys. Rev. Lett.* **1996**, *77*, 3865–3868.
- Pan, L.; Liu, H. J.; Wen, Y. W.; Tan, X. J.; Lv, H. Y.; Shi, J.; Tang, X. F. *Phys. Lett. A* **2011**, *375*, 614–619.
- Spataru, C. D.; Ismail-Beigi, S.; Benedict, L. X.; Louie, S. G. *Phys. Rev. Lett.* **2004**, *92*, 077402.
- Wirtz, L.; Marini, A.; Rubio, A. *Phys. Rev. Lett.* **2006**, *96*, 126104.
- Dean, C. R.; Young, A. F.; Meric, I.; Lee, C.; Wang, L.; Sorgenfrei, S.; Watanabe, K.; Taniguchi, T.; Kim, P.; Shepard, K. L.; Hone, J. *Nat. Nanotechnol.* **2010**, *5*, 722–726.
- Xue, J.; Sanchez-Yamagishi, J.; Bulmash, D.; Jacqu, P.; Watanabe, K.; Taniguchi, T.; Jarillo-Herrero, P.; LeRoy, B. J. *Nat. Mater.* **2011**, *10*, 282–285.
- Ramasubramaniam, A.; Naveh, D.; Towe, E. *Nano Lett.* **2011**, *11*, 1070–1075.
- Otani, M.; Okada, S. *Phys. Rev. B* **2011**, *83*, 073405.
- Tang, K. C.; Gao, Z. X.; Yu, D. P.; Lu, J. unpublished work
- Farmer, D. B.; Golizadeh-Mojarad, R.; Perebeinos, V.; Lin, Y. M.; Tulevski, G. S.; Tsang, J. C.; Avouris, P. *Nano Lett.* **2009**, *9*, 388–392.
- Barraza-Lopez, S.; Vanevic, M.; Kindermann, M.; Chou, M. Y. *Phys. Rev. Lett.* **2010**, *104*, 076807.
- Schwierz, F. *Nat. Nanotechnol.* **2010**, *5*, 487–496.
- Yan, Q.; Huang, B.; Yu, J.; Zheng, F.; Zang, J.; Wu, J.; Gu, B.-L.; Liu, F.; Duan, W. *Nano Lett.* **2007**, *7*, 1469–1473.
- Li, H.; Yan, X.; Luo, G.; Qin, R.; Liu, Q.; Yu, L.; Xu, C.; Zheng, J.; Zhou, J.; Lu, J.; Gao, Z.; Nagase, S.; Mei, W. N. *J. Phys. Chem. C* **2010**, *114*, 15816–15822.
- Marini, A.; García-González, P.; Rubio, A. *Phys. Rev. Lett.* **2006**, *96*, 136404.
- Wang, X.; Ouyang, Y.; Li, X.; Wang, H.; Guo, J.; Dai, H. *Phys. Rev. Lett.* **2008**, *100*, 206803.
- Xia, F.; Farmer, D. B.; Lin, Y.; Avouris, P. *Nano Lett.* **2010**, *10*, 715–718.
- Guzmán-Verri, G. G.; Lew Yan Voon, L. C. *Phys. Rev. B* **2007**, *76*, 075131.

NOTE ADDED IN PROOF

After submission of the manuscript, we became aware of a pioneer theoretical work on silicene (ref 39).